Electronic Supplementary Material (ESI) for Journal of Materials Chemistry A.

Supporting Information

Porous polyaminoamides via an exotemplate synthesis approach for ultrahigh multimedia iodine adsorption

Mohd.Avais and Subrata Chattopadhyay*

Department of Chemistry, Indian Institute of Technology Patna, Bihta, Patna 801103, Bihar, India

** Corresponding authors.*

E-mail addresses: sch@iitp.ac.in

Experimental section

Materials

All starting materials and solvents were obtained from commercial sources and used without further purification. 1, 8-Diaminooctane (≥ 98.0%) was purchased from sigma-Aldrich and N, N′-methylene(bis)acrylamide (bisAcrylamide) 3x crystextrapure AR, THF, ethanol, methanol and n-hexane were purchased from Sisco Research Laboratories Pvt. Ltd.(SRL). Iodine and sodium bicarbonate were bought from Central Drug House (P) Ltd. (CDH). HPLC grade water was used throughout the experiments.

Porous Polymer Synthesis Procedure

The porous polymers were synthesized using $NaHCO_3$ as an exotemplate. Firstly, the aza-Michael addition reaction between octyldiamine (B4 monomer) and bisacrylamide (A2 monomer) in water results the formation of a hyperbranched polymer. The $NaHCO_3$ was then added to the insitu formed hyperbranched polymer solution. Next, the hyperbranched polymer was crosslinked, resulting in the formation of a network structure. During crosslinking, $NaHCO_3$ was entrapped in the polymer networks. The network structure was then kept for lyophilization, followed by heating at ~ 100°C for ~15h. During heating, the $NaHCO_3$ partly decomposed into Na_2CO_3 and CO_2, where the CO_2 evaporated and the Na_2CO_3 remained in the networks. In addition, the final product was then washed thoroughly (3–4 times) with warm water to completely remove the entrapped Na_2CO_3, $NaHCO_3$ (unreacted template) and unreacted monomers. After that, the water was removed by freeze drying to obtain the final porous polymer. Using this method, five different porous polymers (PP-1, PP-2, PP-3, PP-4, and PP-5) were synthesized using varying amounts of $NaHCO_3$ (10, 20, 25, 30, and 40% weight percent). More details are given in table S1.

Table S1: Details of the reagents used for the preparation of porous polymers.

Samples	N,N′-methylene(bis)acrylamide	Diamines (mmol)	Solvent (mL)	Amount of $NaHCO_3$ (weight%)
PP-1	1 g (6.48mmol)	467.9mg (3.24 mmol)	Water (10 mL)	10
PP-2	1 g (6.48mmol)	467.9mg (3.24 mmol)	Water (10 mL)	20
PP-3	1 g (6.48mmol)	467.9mg (3.24 mmol)	Water (10 mL)	25
PP-4	1 g (6.48mmol)	467.9mg (3.24 mmol)	Water (10 mL)	30
PP-5	1 g (6.48mmol)	467.9mg (3.24 mmol)	Water (10 mL)	40

General characterization

Fourier transform infrared (FT-IR) spectra were obtained using a Perkin Elmer spectrum 400 FT-IR with a universal KBr mode accessory. FT-IR data are reported with a wave number range of 500−4000 cm^{-1} with 8 scan.

Solid state ^{13}C NMR spectra were recorded using Jeol NMR ECZ 500 MHz. Carbon chemical shifts are expressed in parts per million (δ scale).

Thermogravimetric analyses (TGA) were carried out on a Q6OO SDT, TA analyzer under an N_2 atmosphere at a heating rate of 10ºC min^{-1} within a temperature range of 30−800°C**.**

Scanning Electron Microscopy (SEM) Surface morphology measurements were executed with a Gemini - 500 Zeiss (Germany) scanning electron microscope with energy-dispersive X-ray spectroscopy (EDX). All the porous polymer samples were freeze dried before analysis. To avoid charging during SEM analyses, we coated all the porous polymer samples with a thin layer of gold by spin coater prior to analyses.

Transmission Electron Microscopy (TEM) analyses were performed using a JEOL TEM at an accelerating voltage of 200 kV. The TEM Samples were prepared for analyses by drop casting the porous polymer samples (dispersed in ethanol) on carbon grids TEM Window (TED PELLA, INC. 200 meshes Cu).

N_2 adsorption desorption analyses were performed at 77 K using a liquid nitrogen bath (77 K) on a QuantachromeQuadrasorb automatic volumetric instrument. Prior to the gas adsorption studies, the entire freeze-dried porous polymer samples were outgassed for 12h at 120°C under vacuum.The surface areas were determined using the Brunauer-Emmett-Teller (BET) model, applied between P/P0 values of 0.05 and 0.35. The pore size distributions were calculated using the non-localized density functional theory (NLDFT) and Barrett-Joyner-Halenda(BJH) method.

UV-vis spectra were obtained using Shimadzu UV 2550 Spectrophotometer.

Raman spectra were obtained using Micro- Raman spectrophotometer (STR 750 RAMAN spectrograph, Seki Technotron Corporation Japan). Raman measurements were done using 633 nm He-Ne lasers.

Mercury intrusion porosimetry (MIP) Meso and macro pores of porous polymers were calculated using Mercury intrusion porosimeter model PM-60 from Quantachrome instruments. A wide range of pore diameters between 950 µm and 0.004 µm were analyzed by applying corresponding equivalent pressures on mercury between 0.1 kPa and 413 MPa. The intruded porosity and pore size distribution were analyzed using the Autopore IV 9500V1.09 standard software package.

To implement the experiment, a freeze-dried porous polymer sample was inserted into the MIP penetrometer, followed by mercury injected into the specimen with pressure.

Ritter and Drake have described a direct method for measuring pore information, including pore volume, porosity, pore size distribution and total intruded mercury volume using a high-pressure mercury porosimeter.[1] When a liquid meniscus is in equilibrium in a cylinder capillary tube of diameter D and there is a pressure difference across the meniscus of magnitude P, then they are connected by the following Washburn equation as.[2]

$$P = \frac{4\gamma\cos\theta}{D} \quad \text{..... (S1)}$$

Where γ is the mercury surface tension and θ is the wetting contact angle between the solid and the mercury, set as 140°.[3]

The pore size distribution is determined from the volume intruded at each pressure increment. Total porosity is determined from the total intruded mercury volume using following equation.[4]

$$\textbf{Total porosity (\%)} = \frac{\textbf{Intruded mercury volume}}{\textbf{Total bulk volume of the material}} \times 100 \quad \text{…….. (S2)}$$

X-ray photoelectron spectroscopy (XPS) spectra were measured on a ULVAC PHI/PHI5000 Versa Probell with an Al monochromatic X-ray source (1486.71 eV).

Iodine adsorption experiments

In vapour phase 10 mg of freeze dried porous polymer samples in an open pre-weighted flat bottom flask (25 mL) and an excess amount of iodine beads were placed in a sealed cylindrical glass vial (approx. 100 mL), then they were sealed at 80°C under ambient pressure in an air-dry oven. The system was cooled down to room temperature and weighted at regular intervals. The adsorption capacity of I_2 for dried porous polymers was determined using the following equation (S3).

$$\mathbf{Q_e = (m_2 - m_1) / m_1 \times 100\ wt\%} \quad \text{……(S3)}$$

Where m_1 is the mass of porous polymer before adsorption, m_2 is the mass of porous polymer after iodine adsorption; Q_e is adsorption capacity of I_2 over porous polymer

Iodine adsorption in organic medium In the current work, we determined the adsorption capacity of the synthesized porous polymers with iodine in solution (n-hexane). Typically, an accurately weighed 10 mg of PPs was added to 10 mL of each iodine solution (concentration 1000 to 5000 ppm). Then the resulting mixture was added into a 20 mL vial and stirred at 600 rpm in a closed condition at room temperature until equilibrium was reached. Furthermore, a 3 mL portion of the aliquot was taken from the mixture and centrifuged instantly for a few minutes to remove the iodine adsorbed porous polymers from the suspension.

The equilibrium adsorption capacity (Q_e) can be determined using the following equation.

$$\mathbf{Q_e = [(C_o - C_e) \times V]/ M} \quad \text{……(S4)}$$

$$\mathbf{Adsorption\ efficiency\ (\%) = [(C_o - C_t)/C_o] \times 100} \quad \text{……(S5)}$$

Where C_o and C_e (mg L^{-1}) are the initial and equilibrium concentration (after adsorption) of the iodine in the stock solution, C_t is the concentration of the iodine solution at time (t), M (g) is the weight of freeze dried porous polymers, V is the total volume of iodine solution in litter.

Iodine adsorption aqueous medium

Before the iodine adsorption studies in water, the I_3^- solutions were prepared by sonicating an equal amount of potassium iodide (KI) and iodine (I_2) in water. Typically, an accurately 2.5 mg of PPs was dipped to 10 mL of each iodine solution (concentration 0.5 mM to 5 mM). Then the resulting mixture was added into a 15 mL vial and stirred at 500 rpm in a closed condition at ambient condition until equilibrium was attained. Furthermore, a 2 mL portion of the aliquot was taken from the mixture and centrifuged instantly for a few minutes to remove the adsorbent from the suspension and the filtrate concentration was analysed by UV−vis measurements to determine the equilibrium adsorption capacity using equation (S4) and (S5).

Titration experiments

2 mg of PPs porous polymers were immersed for 24h at ambient condition in a 10 mL aqueous solution containing 8.3 mg KI and 12.7 mg I_2. The leftover polymers was then filtered and extensively washed with water and ethanol before being vacuum dried. The filtrates were collected and titrated with a 2 percent aqueous starch solution as an indicator against a 0.05 (M) sodium bisulfite solution. The resultant solution contains 4.34 mg, 1.17 mg, 1.01 mg, 2.6 mg, and 4.77 mg I_2 after treated with PP-1, PP-2, PP-3, PP-4 and PP-5 as per calculation. Hence, I_2 adsorption by 2 mg of PP-1, PP-2, PP-3, PP-4 and PP-5 are 8.35 mg, 11.52 mg, 11.68 mg, 10.1 mg, and 7.92 mg, respectively. Therefore, the capacity of I_2 adsorption by PP-1, PP-2, PP-3, PP-4 and PP-5 in water are 4.17 g/g, 5.76 g/g, 5.84 g/g, 5.05 g/g, and 3.96 g/g.

Reversibility Studies

a. In vapor phase

Iodine release and adsorbent recycle upon heating were conducted as follows: 15 mg of iodine adsorbed PP-3-I_2 polymer was charged in an open glass vial and heated at

140℃ in the air oven. The iodine release efficiency was determined using weight losses equation.

$$\mathbf{I_R = (15\text{-}m_t)/m_i \times 100\ wt\%\ .....(S6)}$$

Where, I_R is the iodine release efficiency, m_t is the weight of the PP-3 after heating release at different time interval, and m_i was weight of adsorbed iodine in 15 mg of iodine-equilibrium PP-3-I_2 polymer.

b. In solution phase

Iodine release and adsorbent recycle in solution were investigated as follows: 5 mg of iodine-equilibrium PP-3-I_2 polymer was immersed in methanolic solution of tetrabutylammonium bromide at ambient conditions. The iodine released was observed using UV−vis spectroscopy at various time intervals.

Selectivity studies

The effects of pH on the uptake of I_3^- were investigated by adjusting the pH from 4 to 9.2 with buffer solutions. In the selectivity experiment, 1 mg of PP-3 was immersed individually into a binary solution which containing 5 mL of I_3^- solution (concentration 5 mM) and 5 mL each of various competing anions solution (NO_3^-, Cl^-, CH3COO$^-$, Br^-, SO_4^{2-}, and F^-) (concentration 5 mM). For 24h, the final mixture was stirred at 500-600 rpm in a sealed container at room temperature. Then, equilibrium was attained, supernatant was taken, and the supernatant concentration was measured by UV−vis spectroscopy. The efficiency of the iodine adsorption in the presence of others anions were analysed with respect to a blank solution where 5 mL of distilled water is used instead of other anions solution. The adsorption capacity was determined from the initial and final absorbance of the supernatant by equation S4 and S5. The same procedure also applied for iodine adsorption experiment in the presence of a mixture of competing ions.

K_d Calculation Formula

$$k_d = (C_1 - C_2)/C_2 \times V/M \text{ …….. (S7)}$$

The distribution coefficient values were determined by the formula used in equation (S7). Herein, K_d is the distribution coefficient, C_2 and C_1 represents the final and initial concentration, respectively. V represents the volume of the total solution, while M is the weight of the adsorbent.

Table S2: The calculated K_d value of PPs in both media (water and n-hexane).

Samples	K_d values in water (mL/g)	K_d values in n-hexane (mL/g)
PP-1	3.9×10^3	1.5×10^3
PP-2	8.9×10^3	2.4×10^3
PP-3	9.4×10^3	3.7×10^3
PP-4	6.3×10^3	1.9×10^3
PP-5	3.7×10^3	1.2×10^3

Seawater Experiment

Before the iodine adsorption studies in seawater, the basic and complex seawater solutions were prepared in the laboratory using table salt and other various salts. Typically, an accurately weighed 2.5 mg of PP-3 was immersed into 10 mL of each iodine solution (in basic and complex sea water, concentration of 5 mM). For 24h, the final mixture was stirred at 500-600 rpm in a sealed container at room temperature. Then, equilibrium was attained, the supernatant was taken, and the supernatant concentration was investigated by UV−vis spectroscopy. The maximum adsorption capacity was determined from the initial and final absorbance of the supernatant by equations S4 and S5.

Adsorption isotherm models

The adsorption isotherm behaviour of the porous polymer for iodine was investigated using the Langmuir and Freundlich adsorption isotherm models.

The Langmuir isotherm model The Langmuir isotherm is presented by the following equation (S8)

$$Q_e = Q_m K_L C_e/(1+K_L C_e) \text{ ……....(S8)}$$

Where Ce (mg L^{-1}) is iodine concentration at equilibrium, Q_e (mg g^{-1}) denote the equilibrium adsorption capacity. Q_m (mg g^{-1}) is the maximum adsorption capacity of the porous polymer for iodine and K_L (mg L^{-1}) is Langmuir adsorption constant that indicate binding energy of adsorption

The Freundlich isotherm model The Freundlich isotherm model described by the following equation (S9)

$$Q_e = K_F C_e^{1/n} \quad \text{.....(S9)}$$

Where C_e (mg L^{-1}) is iodine and dyes concentration at equilibrium, Q_e (mg g^{-1}) denote the equilibrium adsorption capacity K_F and n are the adsorption capacity and the adsorption intensity constant for Freundlich adsorption isotherm model.

Iodine adsorption kinetic studies

To investigate the adsorption kinetics of iodine by the PP-3 polymer, pseudo-first-order (S10) and pseudo-second-order (S11) rate equations were used to understand the mechanism of the iodine adsorption process. Their corresponding linear equations are presented as below:

$$\ln (q_e - q_t) = \ln q_e - k_1 t \quad \text{..... (S10)}$$

$$\frac{t}{q_t} = \frac{1}{k_2 q_e^2} + \frac{t}{q_e} \quad \text{.....(S11)}$$

Here, q_e and q_t represents to the amount of iodine adsorption (mg g^{-1}) at equilibrium and the amount of iodine adsorbed (mg g^{-1}) at any given time t respectively. k_1 (min^{-1}) and k_2 are the pseudo-first-order and the pseudo-second-order rate constants for adsorption kinetic behavior.

Irradiation experiment

The irradiation experiments of PP-3 polymer were performed via different irradiations using sunlight for 5 days, includes 60h (temperature 32-39°C, humidity 55-70%, wind speed 8-14 km/h, 27.35mW/cm^2 intensity*), UV radiation (365 nm wavelength[#]) for 24h, X-ray for 3h (a voltage of 45kV using Cu Kα radiation, λ= 0.15418 nm) and ^{60}Co gamma-ray irradiation at 200kGy (with a dose rate of 1.95kGy/h) under an air atmosphere. The molecular structure and surface morphology of post-treated samples was analyzed via IR, solid ^{13}C-NMR, and FESEM. Further, their iodine adsorption performance in multi phases (vapor, organic and aqueous) was also investigated.

*** Calculation of sunlight intensity using pyranometer**

Model: CMP-11 (Kipp & Zonen USA Inc.)

At highest temperature (I_1)

Instrument reading (ir) = 2.9 mV

Sensitivity = 9.62μV/W/m^2

Intensity = ir × [1000/Sensitivity] = 2.9 × [1000/9.62] = 301.45 W/m^2 = 30.14mW/cm^2

Similarly calculated at medium temperature I_2 **(**27.02mW/cm^2**)** and lowest temperature I_3 (24.94mW/cm^2)

Average intensity = (I_1 + I_2 + I_3)/3 = (30.1 + 27.02 + 24.94)/3 = 27.35 mW/cm^2

The UV unit was consisted of fourteen 8W low-pressure mercury lamps of 20cm length, housed in an enclosed stainless steel cabinet (LZC-4X, Luzehem) with internal dimensions of 32 x 33 x 21 cm (W x D x H).

Figures-

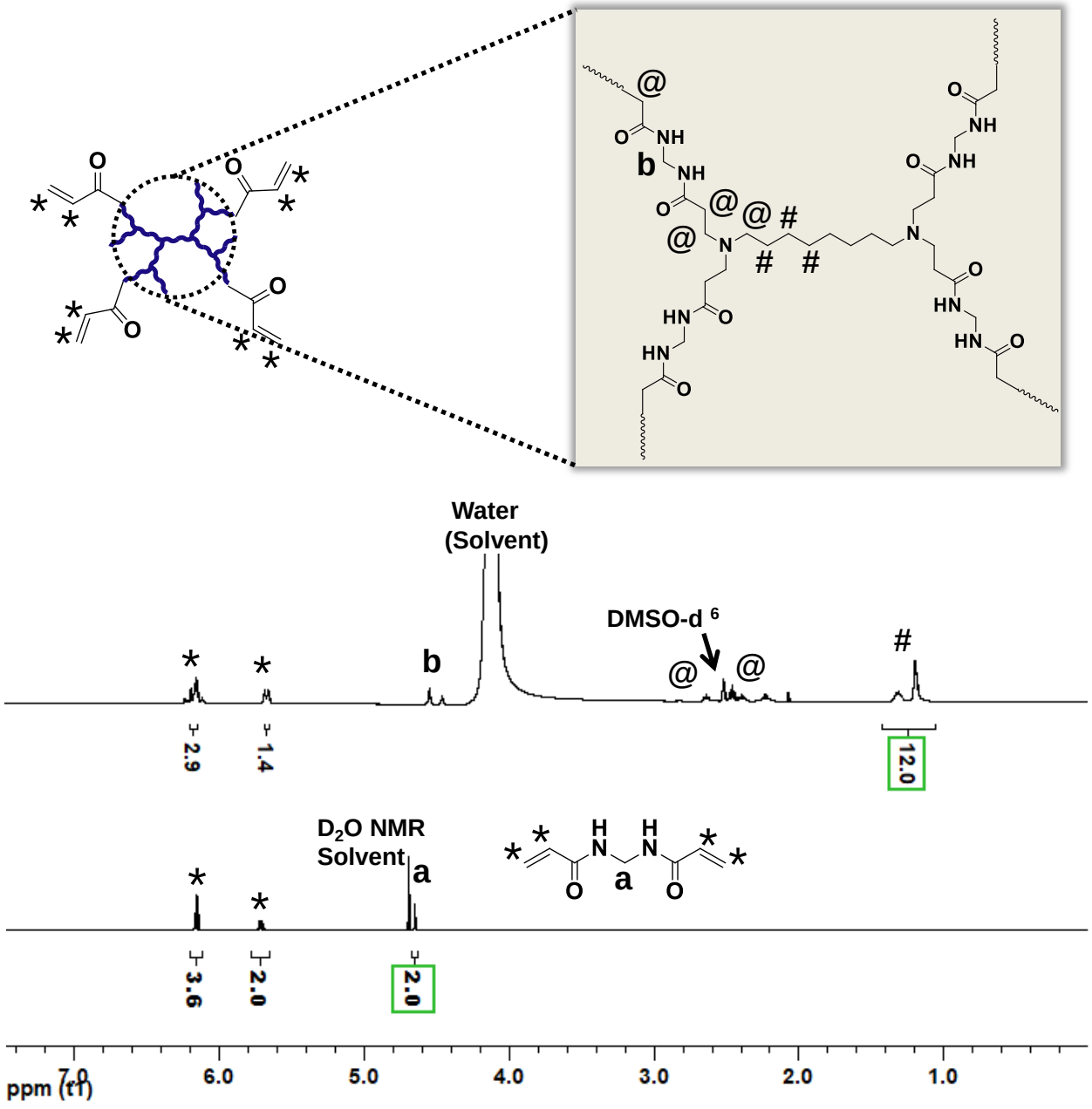

Figure S1: ^{1}H NMR spectrum of hyperbranched polymer.

Table S3: Results of the SEC (coupled with triple detectors) analysis of the hyperbranched polymer (analysis performed byASTRA 7.3.0 software -Wyatt Technology Corporation).

Samples	M_n(g/mol)	M_w (g/mol)	PDI (M_w/M_n)	r_h(v)z (nm)	Rz (RMS) (nm)	Exponent of Mark Houwink plot	Exponent of Conformation plot
HBP	1.519×10^7	3.005×10^7	1.97	140.5	74.6	0.186	0.002

* abnormal due to hyperbranched polymer-columninteraction/bigger size.

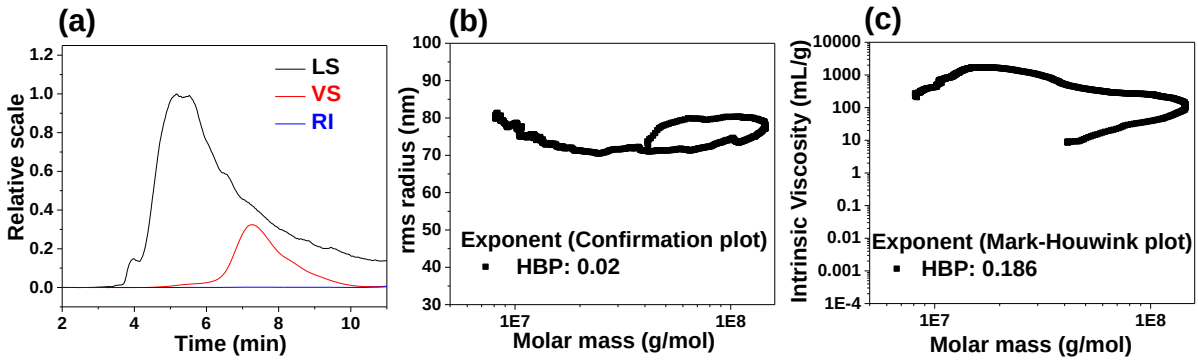

Figure S2: SEC analysis of HBP with (a) chromatograms with LS, VS and RI detectors (b) conformation plot and (c) Mark-Houwink plot revealing the hyperbranched architecture.

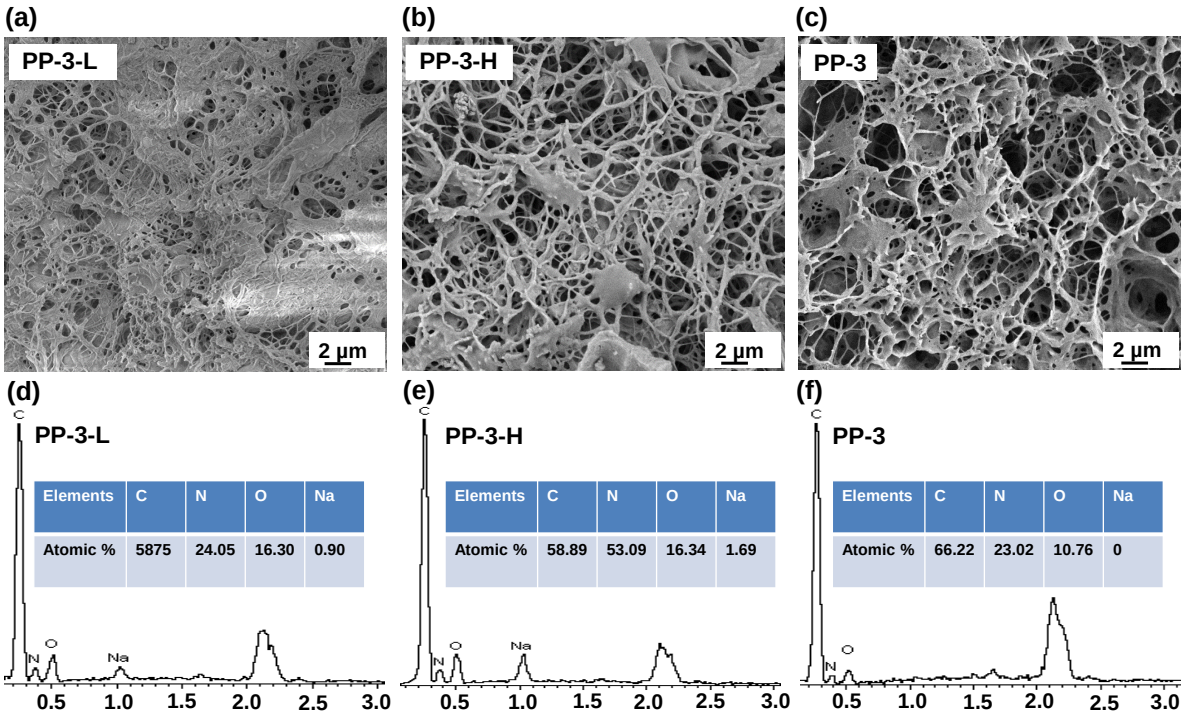

Figure S3: SEM micrograms of (a) PP-3-L (after lyophilization), (b) PP-3-H (after lyophilization & heating) and (c) PP-3 (after lyophilization, heating and washing) – showing the crosslinked porous structure, and (d, e, and f) EDX line graph of PP-3-L, PP-3-H, and PP-3, respectively.

Table S4: Porosity and surface area analysis of PPs.

Samples	Total Pore Volume ($V_{1.0}$, NLDFT) (cc/g)	Total Pore Volume ($V_{1.0}$, BJH) (cc/g)	Average Pore size (NLDFT) (nm)	Average Pore size (BJH) (nm)	Micropore volume by DR method (cc/g)	$V_{0.1}$ (cc/g)	Micropore content $V_{0.1}/V_{total} \times 100\%$	Mesopore content $(V_{total} - V_{0.1})/V_{total} \times 100\%$	Total Intruded pore volume by MIP (cc/g)	Surface area (m^2/g)	Porosity % (MIP)
PP-1	0.071	0.098	2.76	2.76	0.011	0.019	19.4	80.6	1.78	65	63
PP-2	0.106	0.145	3.16	2.20	0.016	0.030	20.6	79.6	2.55	103	83
PP-3	0.144	0.195	3.16	2.75	0.021	0.041	21.0	79.0	2.89	146	93
PP-4	0.085	0.124	4.54	3.07	0.011	0.022	17.7	82.3	1.91	76	67
PP-5	0.070	0.077	3.16	3.42	0.005	NA	NA	NA	1.37	60	56

* The level of microporosity in the materials was assessed by the ratio of micropore volume to the total pore volume ($V_{0.1}/V_{total}$).[5-6]

Micropore volume also calculated by Dubinin-Radushkevich (DR) method.

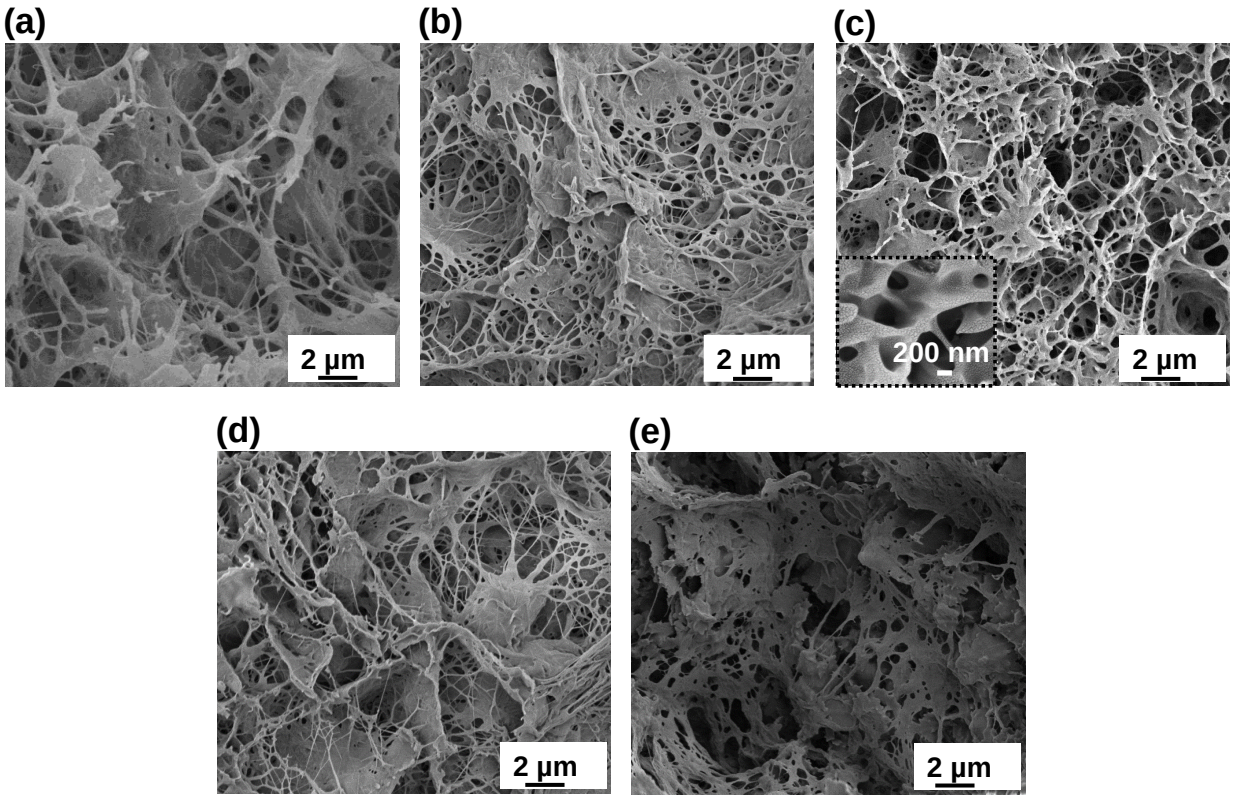

Figure S4: SEM micrograms of (a) PP-1, (b) PP-2, (c) PP-3, (d) PP-4, and (e) PP-5 indicated the presence of mesopores and macropores in the network.

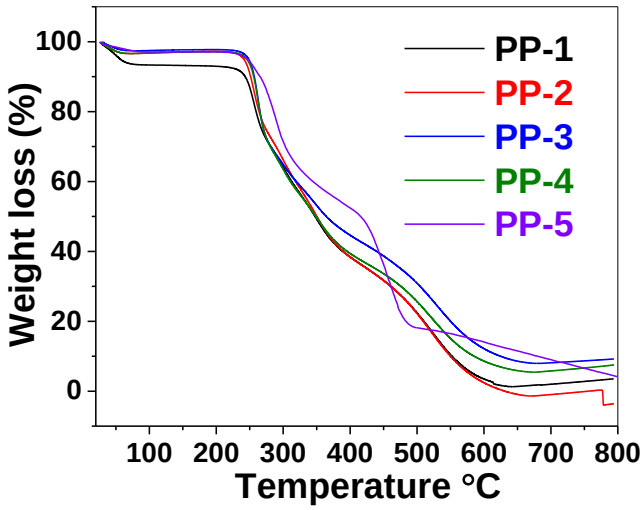

Figure S5: Thermogravimetric analysis of PPs polymers.

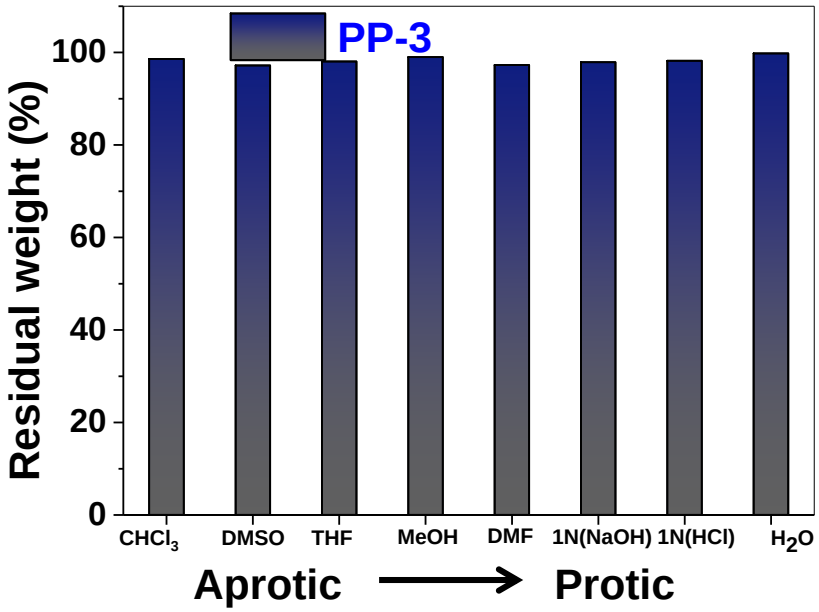

Figure S6: Residual weight percentage plot, of PP-3 after exposure to different solvent.

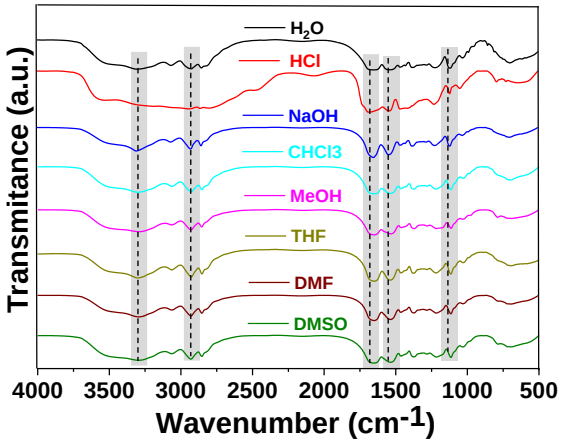

Figure S7: IR spectra, of PP-3 after exposure to different solvent.

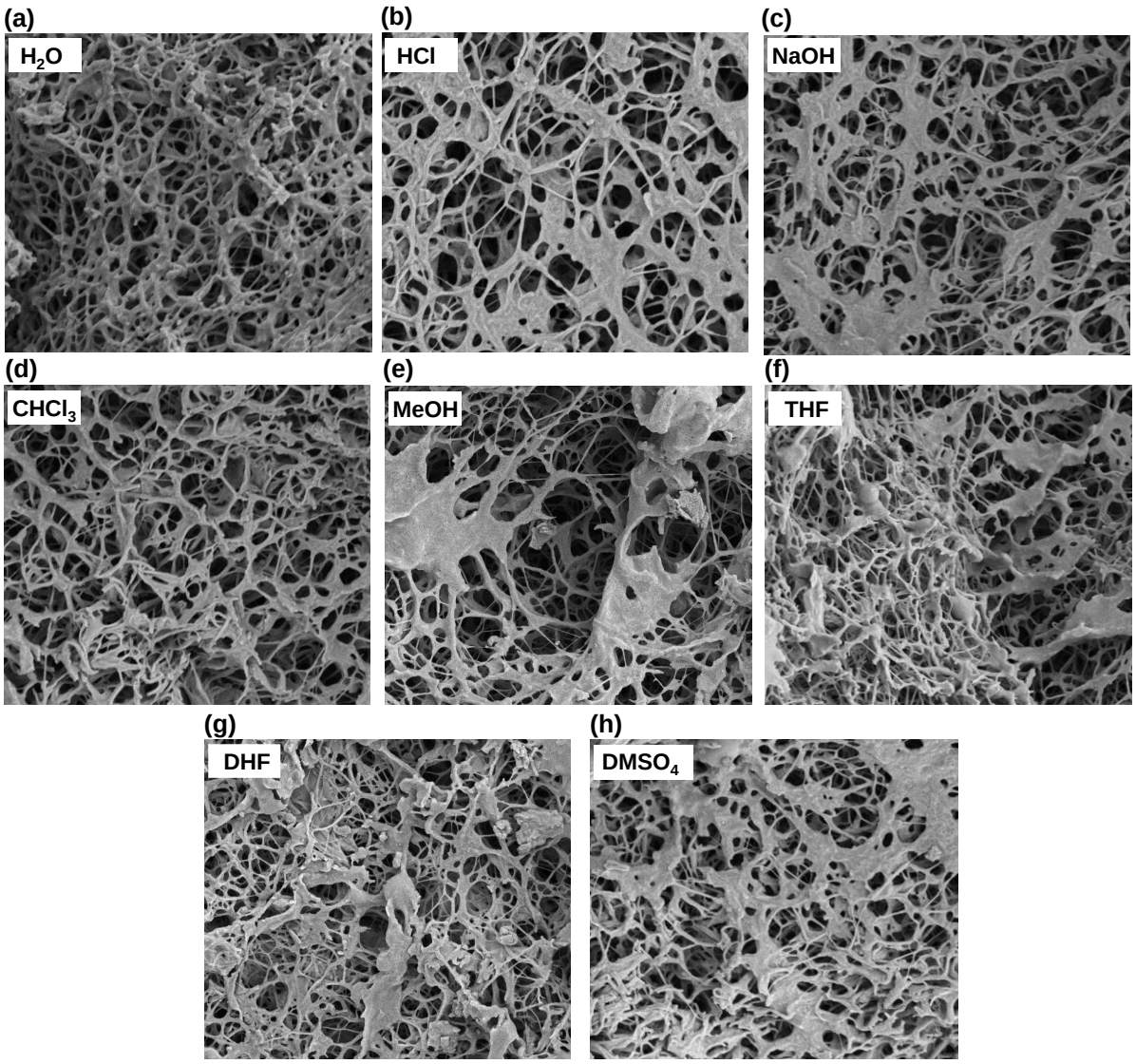

Figure S8: FESEM images of PP-3 after different solvent treatment (a) water, (b) HCl, (c) NaOH, (d) CHCl3, (e) MeOH, (f) THF, (g) DMF, and (h) DMSO.

Table S5: Comparison of the current work with recent literatures in context of iodine adsorption capacity in vapor phase (the best example from the given reference was taken for comparison).

Adsorbents	S_{BET} (m^2 g^{-1})	Adsorption capacity (g/g)	Experiment conditions	References
HKUST-1@PES	1370	5.8	Vapor adsorption, 75°C, ambient pressure	Ref[7]
AlOC-26-NC	508	0.71	Vapor adsorption, 80°C, ambient pressure	Ref[8]
TPT-BDCOF	109	5.43	Vapor adsorption, 75°C, ambient pressure	Ref[9]
BTM	NA	4.46	Vapor adsorption, 75°C, ambient pressure	Ref[10]
CMP-4	9.5	2.08	Vapor adsorption, 75°C, ambient pressure	Ref[11]
CMPN	86.2	5.03	Vapor adsorption, 75°C, ambient pressure	Ref[12]
TPB-DMTP COF	1927	6.2	Vapor adsorption, 77°C, ambient pressure	Ref[13]
iCOF-AB-50	1390	10.21	Vapor adsorption, 75°C, ambient pressure	Ref[14]
JUC-561	2359	8.19	Vapor adsorption, 75°C, ambient pressure	Ref[15]
POPs(TBIM)	8.12	9.43	Vapor adsorption, 77°C, ambient pressure	Ref[16]
PP-3	**146**	**10.13**	Vapor adsorption, 80°C, ambient pressure	**This Work**

* For references, please see the references section given at the end.

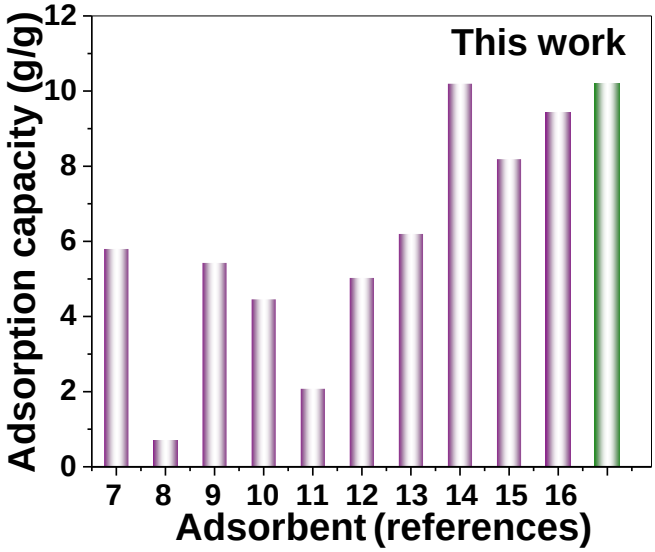

Figure S9: Comparison of the current work with recent literatures in context of iodine adsorption capacity in vapor phase.

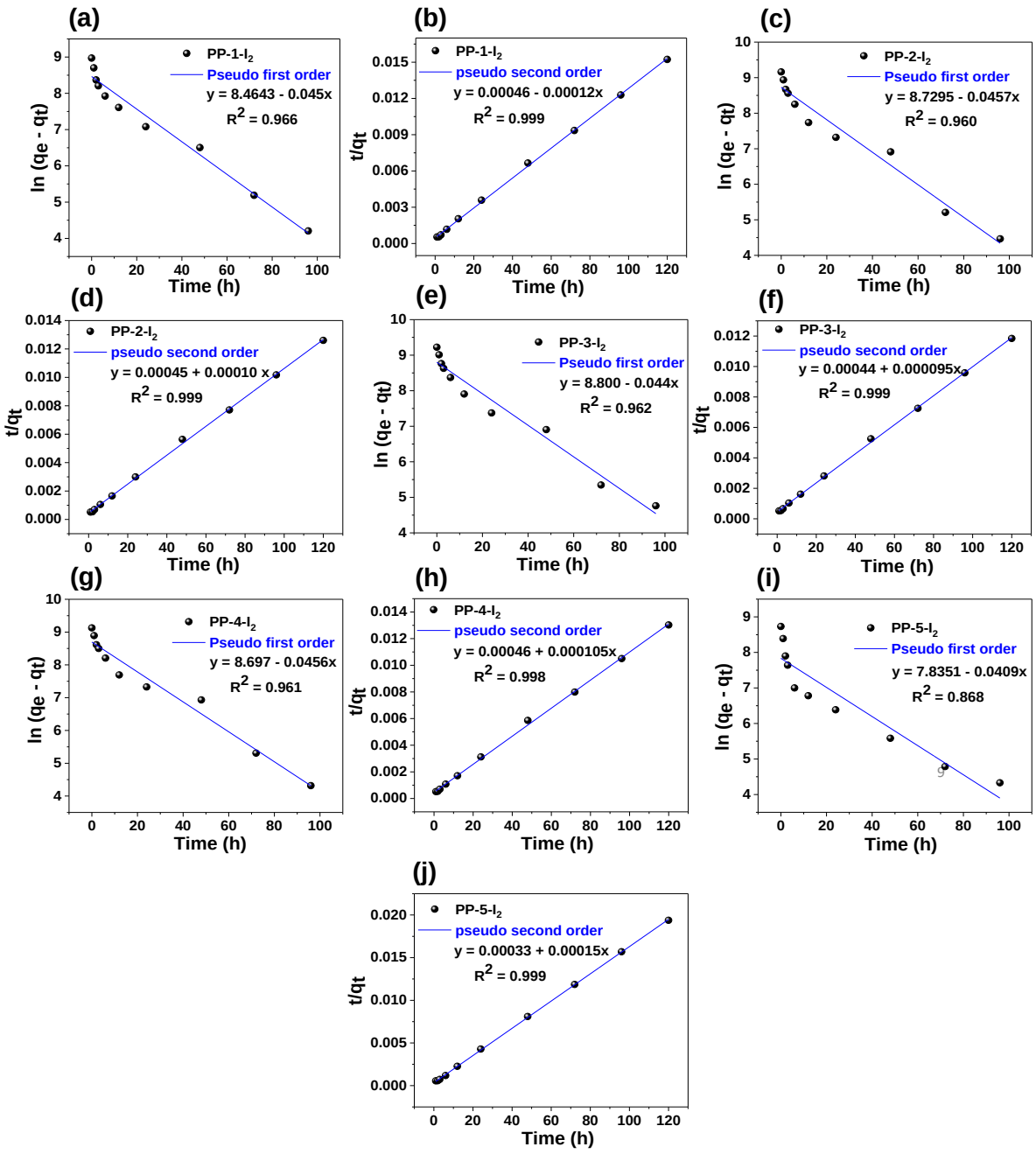

Figure S10: The pseudo-first and second-order model plots for adsorption of I_2 in vapor phase (a and b) for PP-1, (c and d) for PP-2, (e and f) for PP-3, (g and h) for PP-4, (i and j) for PP-5, respectively.

Table S6: Adsorption isotherm parameters of the linear pseudo first order and pseudo second order model for iodine removal by PPs in vapor phase.

		pseudo first order			pseudo second order		
Polymers	$Q_{e,exp}$ (mg g^{-1})	Q_e (mg g^{-1})	k_1(min^{-1})	R^2	Q_e (mg g^{-1})	k_2 (g mg^{-1} min^{-1})	R^2
PP-1	7881	4742.6	0.045	0.96	8084.2	$3.317\times E^{-5}$	0.99
PP-2	9523	6183.0	0.045	0.96	9893.3	$2.287\times E^{-5}$	0.99
PP-3	10134	6639.2	0.044	0.96	10484.3	$2.030\times E^{-5}$	0.99
PP-4	9214	5986.1	0.045	0.96	9496.6	$2.405\times E^{-5}$	0.99
PP-5	6193	2527.7	0.040	0.86	6264.4	$7.701\times E^{-5}$	0.99

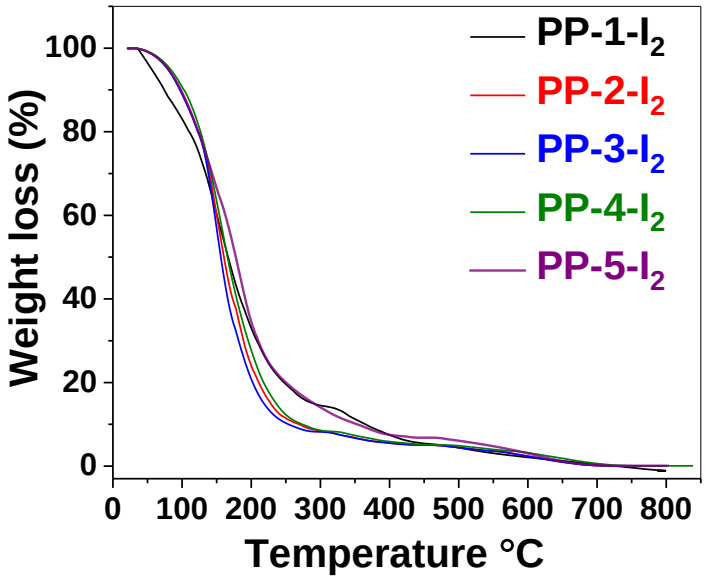

Figure S11: TGA curves of PP-1-I_2, PP-2-I_2, PP-3-I_2, PP-4-I_2 and PP-5-I_2.

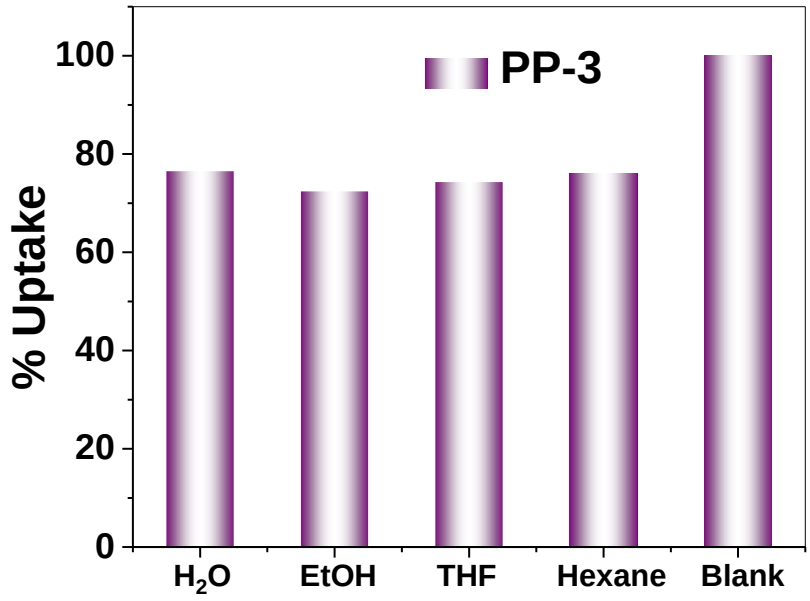

Figure S12: The percentage of iodine vapor uptake in the presence of other aqueous and organic vapors.

Table S7: Comparison of the current work with recent literatures in context of iodine adsorption capacity in organic solvent (the best example from the given reference was taken for comparison).

Adsorbents	**S_{BET} (m^2 g^{-1})**	**Adsorption capacity (g/g)**	**References**
AzoPPN	400	0.735	Ref[17]
FCMP@2	636	0.729	Ref[18]
NRPP-2	1028	0.505	Ref[19]
CSU-CPOPs-1	1032	0.374	Ref[20]
SCMP-2	855	0.249	Ref[21]
TTDP-3	13.20	0.784	Ref[22]
H-C-CTPs	640	0.293	Ref[23]
Complex 1'	762.5	1.01	Ref[24]
DESs	NA	0.99	Ref[25]
1	NA	0.168	Ref[26]
PP-3	**146**	**4.74**	**This Work**

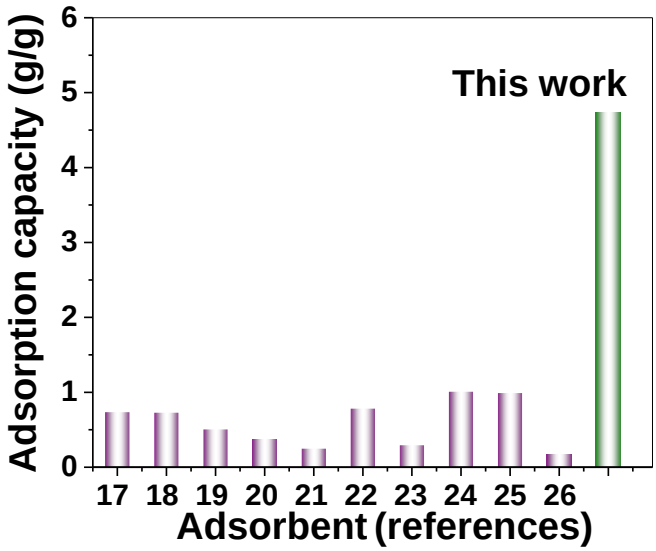

Figure S13: Comparison of the current work with recent literatures in context of iodine adsorption capacity in n-hexane.

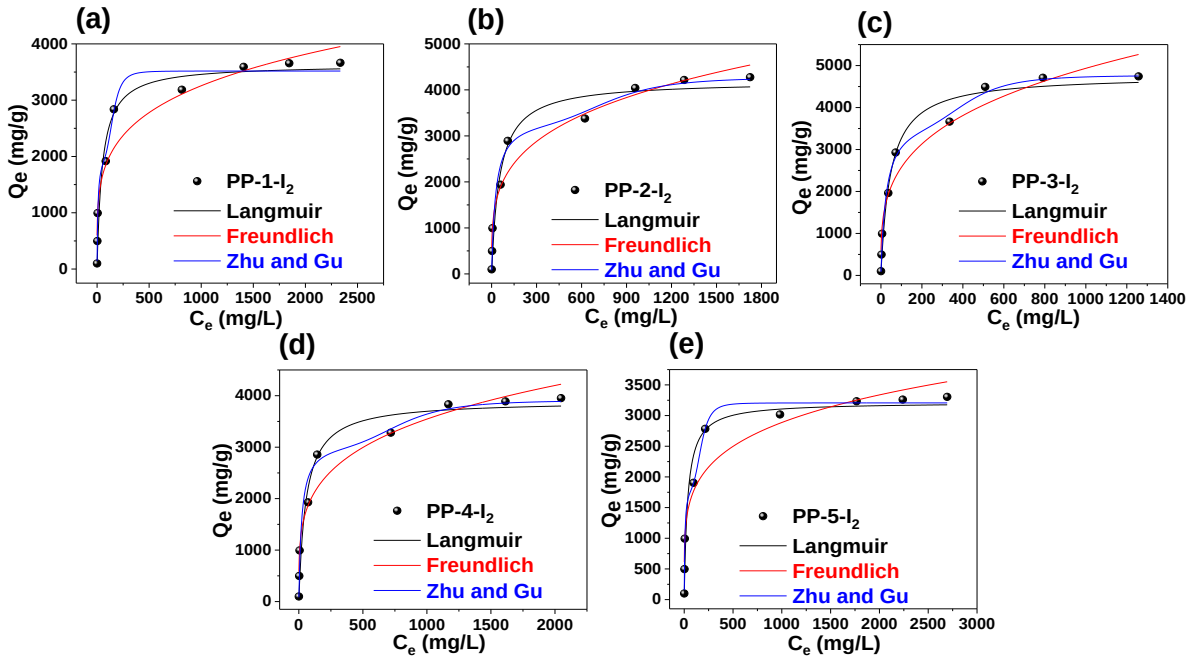

Figure S14: Langmuir, Freundlich and Zhu and Gu adsorption isotherm models for iodine, removal by (a) PP-1, (b) PP-2, (c) PP-3, (d) PP-4 and (e) PP-5, respectively.

Table S8: Adsorption isotherm parameters of the Langmuir and Freundlich model for Iodine removal by PP-1, PP-2, PP-3, PP-4 and PP-5.

		Langmuir model			**Freundlich model**		
Polymers	Adsorbate	Q_m (mg g^{-1})	K_L(L mg^{-1})	R^2	K_F (L mg^{-1})	n	R^2
PP-1	I_2	3633.7	0.019	0.95	671.9	4.37	0.93
PP-2	I_2	4191.7	0.018	0.95	652.2	3.84	0.95
PP-3	I_2	4766.7	0.021	0.97	701.3	3.54	0.94
PP-4	I_2	3901.9	0.018	0.95	657.5	4.09	0.94
PP-5	I_2	3217.2	0.028	0.94	681.6	4.78	0.91

Table S9: Adsorption isotherm parameters of the Zhu and Gu model for iodine removal by PP-1, PP-2, PP-3, PP-4 and PP-5.

		Zhu and Gu model					
Polymers	Adsorbate	Q_m (mg g^{-1})	n	K_1	K_2	K_3	R^2 value
PP-1	I_2	3518.1	5	0.122	$1.704\times E^{-9}$	3	0.98
PP-2	I_2	4272.8	5	0.037	$2.363\times E^{-12}$	4	0.97
PP-3	I_2	4766.9	5	0.039	$2.723\times E^{-11}$	4	0.99
PP-4	I_2	3908.8	5	0.045	$2.231\times E^{-12}$	4	0.97
PP-5	I_2	3206.7	5	0.146	$1.037\times E^{-9}$	3	0.98

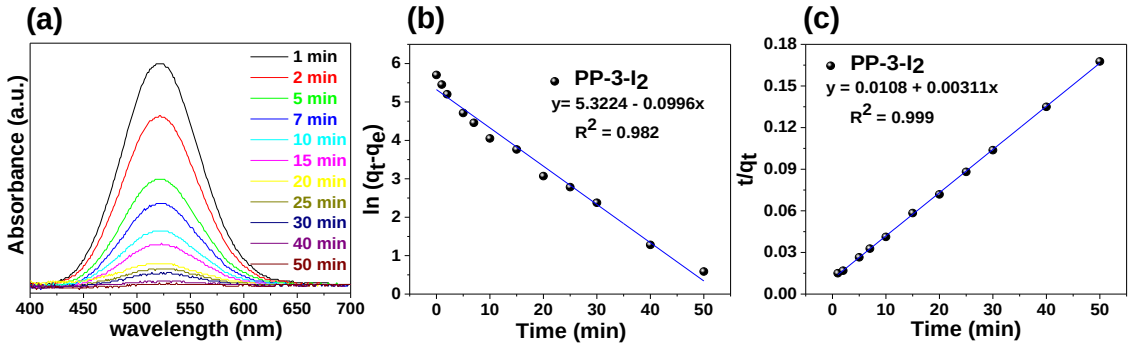

Figure S15: (a) Kinetic study of iodine in n-hexane after being treated with PP-3 by UV-Vis adsorption spectra, (b) the pseudo-first-order, (c) the pseudo-second-order kinetic model plots for adsorption of iodine by PP-3 in n-hexane solution.

Table S10: Pseudo-first-order and pseudo-second-order kinetic parameters for the adsorption of iodine (300 mg/L) in n-hexane by PP-3.

Model	Parameters	Values
Pseudo-first order	Q_e,exp (mg g^{-1})	298.2
	Q_e,cal (mg g^{-1})	204.8
	k_1 (min^{-1})	0.0996
	R^2	0.982
Pseudo-second order	Q_e,cal (mg g^{-1})	321.5
	k_2 (g mg^{-1} min^{-1})	0.00089
	R^2	0.999

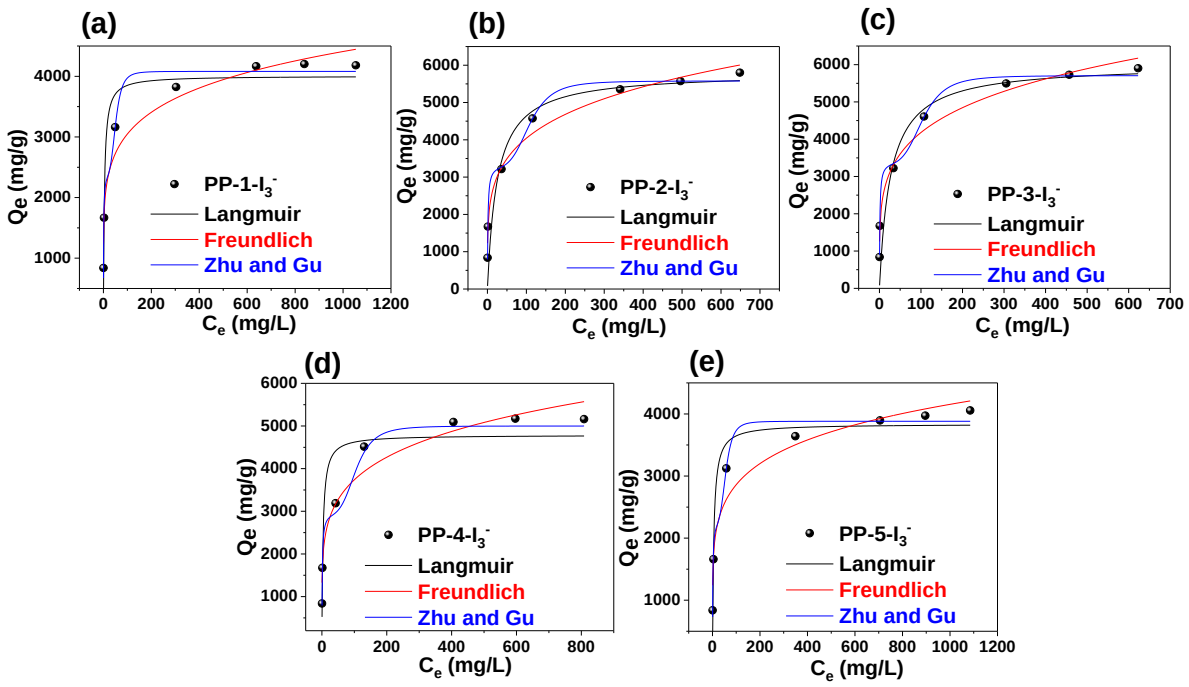

Figure S16: Langmuir, Freundlich and Zhu and Gu adsorption isotherm models for I_3^-, removal by (a) PP-1, (b) PP-2, (c) PP-3, (d) PP-4 and (e) PP-5, respectively.

Table S11: Adsorption isotherm parameters of the Langmuir and Freundlich model for I_3^- removal by PP-1, PP-2, PP-3, PP-4 and PP-5

		Langmuir model			**Freundlich model**		
Polymers	Adsorbate	Q_m (mg g^{-1})	K_L(L mg^{-1})	R^2	K_F (L mg^{-1})	n	R^2
PP-1	I_3^-	4006.2	0.247	0.92	1456.4	6.23	0.94
PP-2	I_3^-	5802.9	0.039	0.86	1525.2	4.72	0.98
PP-3	I_3^-	6001.6	0.037	0.86	1564.3	4.68	0.98
PP-4	I_3^-	4786.4	0.279	0.87	1552.9	5.24	0.95
PP-5	I_3^-	3837.0	0.190	0.94	1355.6	6.16	0.94

Table S12: Adsorption isotherm parameters of the Zhu and Gu model for I_3^- removal by PP-1, PP-2, PP-3, PP-4 and PP-5.

Zhu and Gu model							
Polymers	Adsorbate	Q_m (mg g^{-1})	n	K_1	K_2	K_3	R^2 value
PP-1	I_3^-	4081.2	5	1.052	$1.42\times E^{-7}$	3	0.97
PP-2	I_3^-	5577.9	5	0.861	$6.931\times E^{-9}$	3	0.99
PP-3	I_3^-	5705.4	5	0.990	$8.212\times E^{-9}$	3	0.99
PP-4	I_3^-	5000.00	5	0.813	$8.030\times E^{-9}$	3	0.98
PP-5	I_3^-	3881.7	5	0.789	$9.629\times E^{-8}$	3	0.98

Table S13: Comparison of the current work with recent literatures in context of iodine adsorption capacity in water (the best example from the given reference was taken for comparison).

Adsorbents	**S_{BET} (m^2 g^{-1})**	**Adsorption capacity (g/g)**	**References**
Compound-1	48	3.5	Ref[27]
SCNU-Z4	584.8	3.31	Ref[28]
CaCOP3	81.09	3.1	Ref[29]
CalCOP1	280	2.32	Ref[30]
HCOF-1	NA	2.01	Ref[31]
δ-Bi2O3@PES	10.96	0.170	Ref[32]
Ag-MSHC-6	NA	0.771	Ref[33]
n-CF@OCDs	NA	0.19	Ref[34]
Al-DMAPS	190	0.241	Ref[35]
C-poly-15	96.1	3.2	Ref[36]
PP-3	**146**	**5.90**	**This Work**

* For references, please see the references section given at the end.

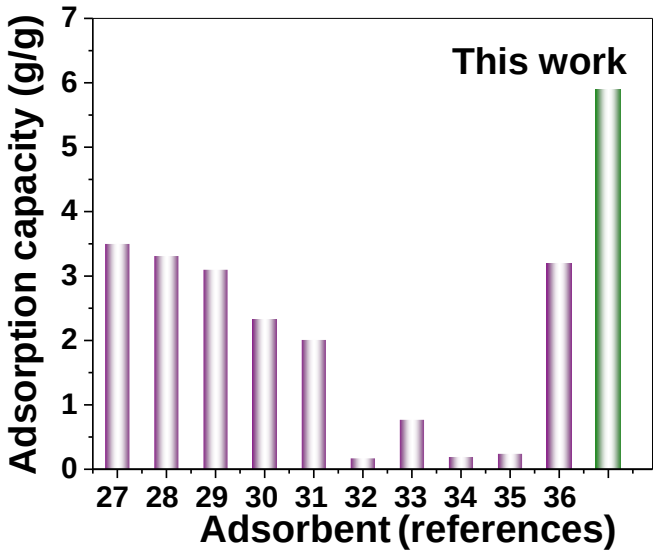

Figure S17: Comparison of the current work with recent literatures in context of triiodide ion adsorption capacity in water.

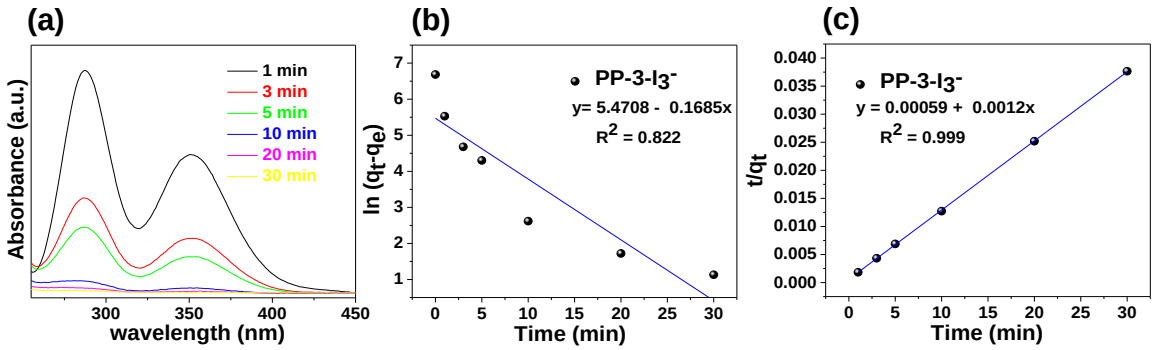

Figure S18: (a) Kinetic study of triiodide in water after being treated with PP-3 by UV-Vis adsorption spectra, (b) the pseudo-first-order, (c) the pseudo-second-order kinetic model plots for adsorption of I_3^- by PP-3 in aqueous solution.

Table S14: Pseudo-first-order and pseudo-second-order kinetic parameters for the adsorption of I_3^- in water by PP-3.

Model	Parameters	Values
Pseudo-first order	Q_e,exp (mg g^{-1})	796.9
	Q_e,cal (mg g^{-1})	237.6
	k_1 (min^{-1})	0.1685
	R^2	0.882
Pseudo-second order	Q_e,cal (mg g^{-1})	813.0
	k_2 (g mg^{-1} min^{-1})	0.00059
	R^2	0.999

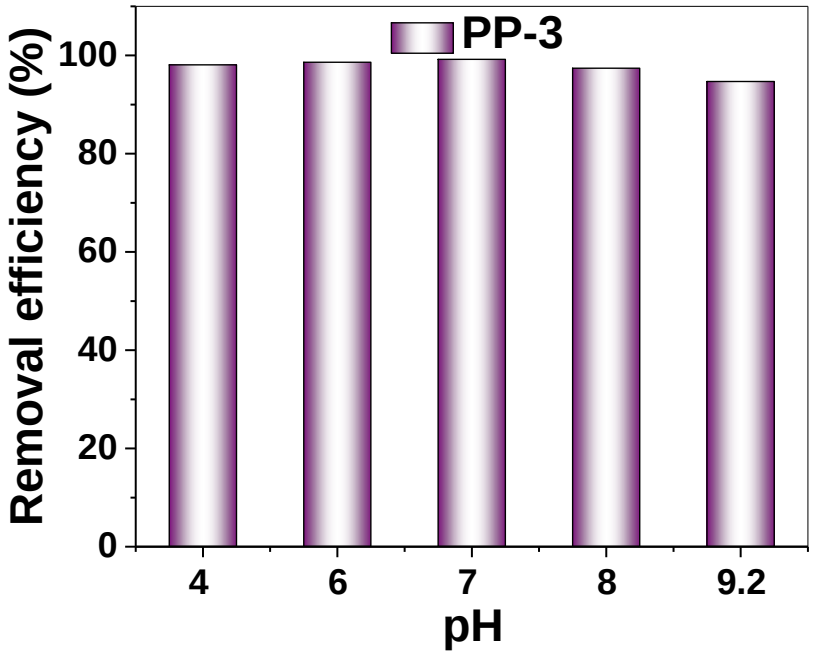

Figure S19: Effect of pH on iodine adsorption by PP-3.

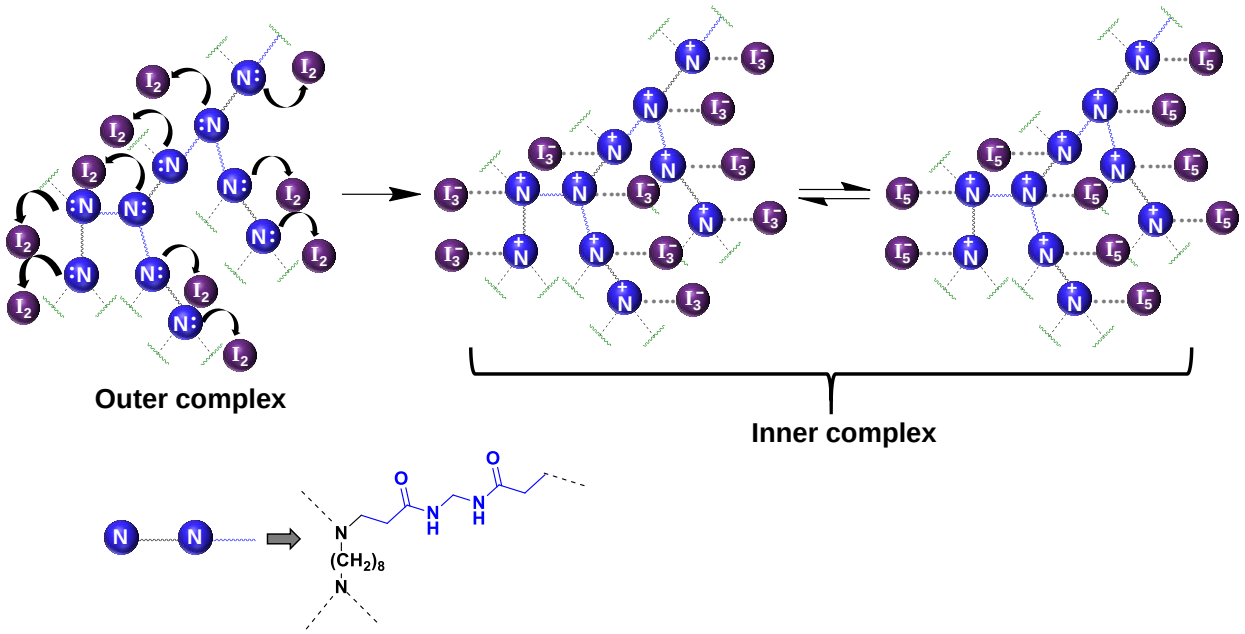

Figure S20: Proposed mechanism for iodine adsorption.

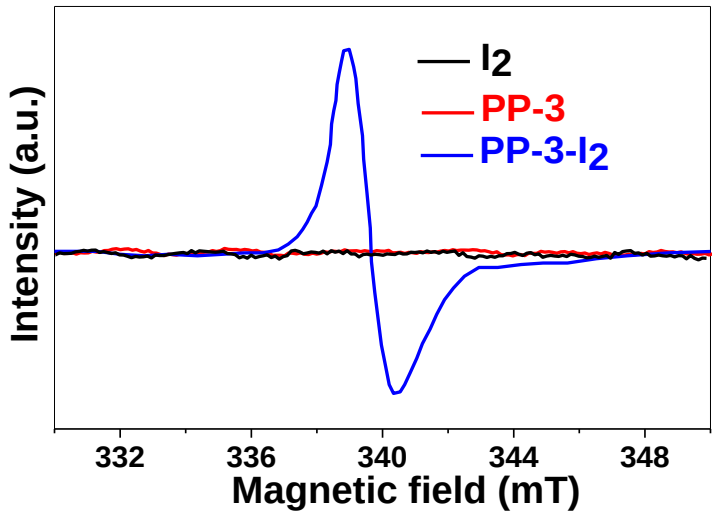

Figure S21: ESR spectra of iodine, before iodine adsorption (PP-3), and after iodine adsorption (PP-3-I_2).

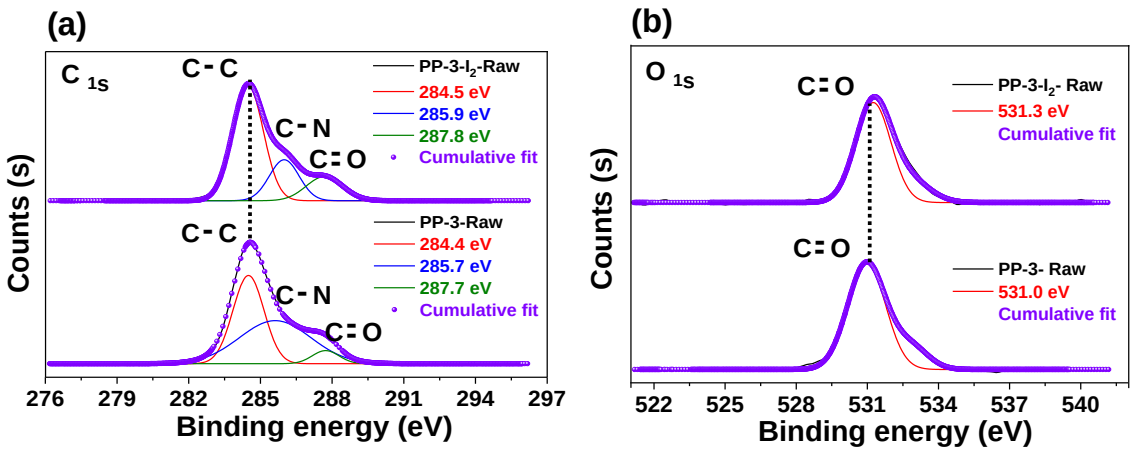

Figure S22: XPS spectra of PP-3 and PP-3-I_2, (a) C 1s, and (b) O 1s.

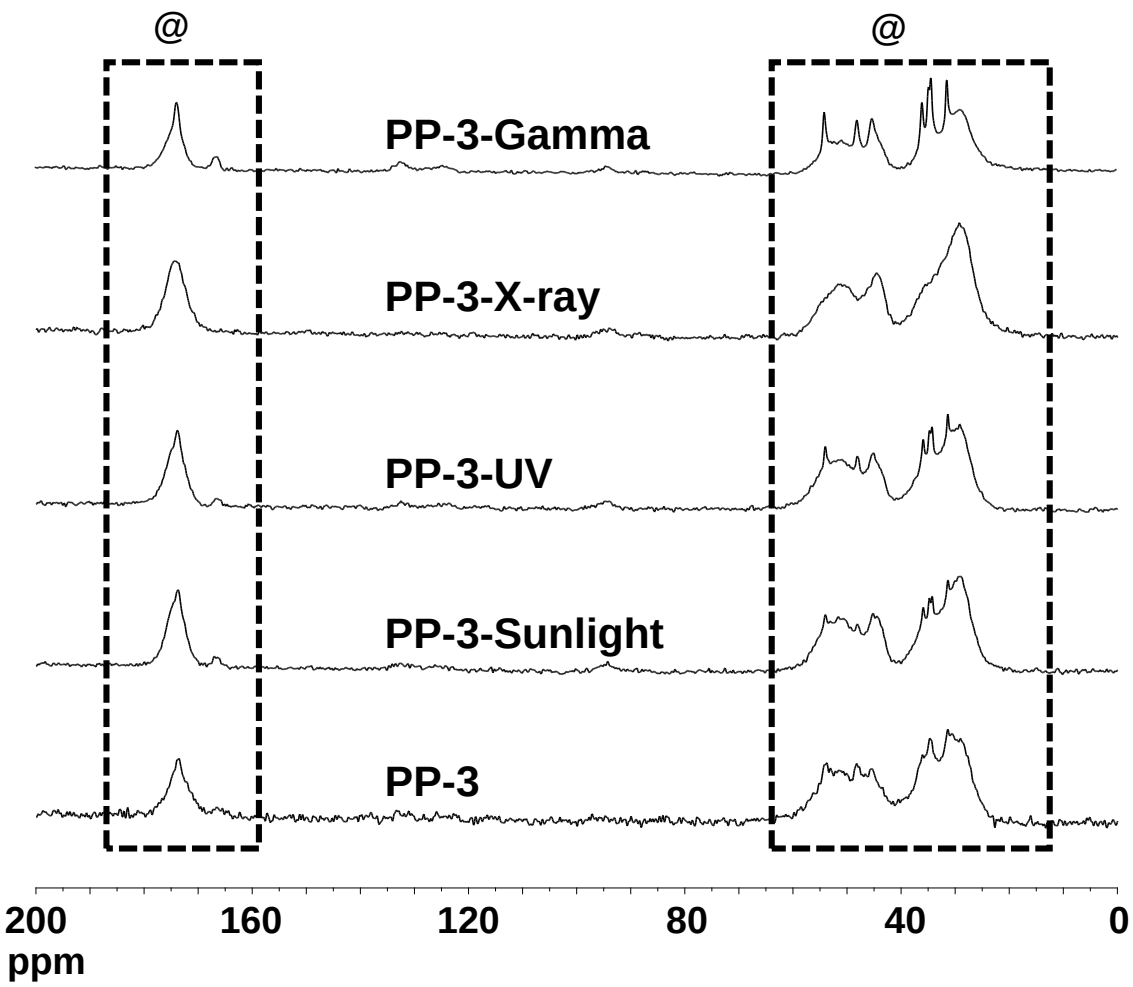

Figure S23: Solid ^{13}C-NMR, of PP-3 after exposure to different radiations.

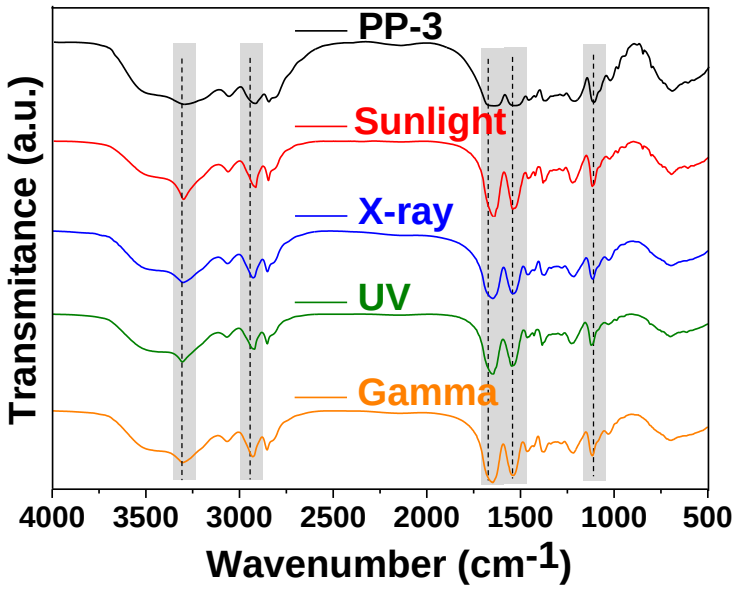

Figure S24: IR spectra, of PP-3 after exposure to different radiations.

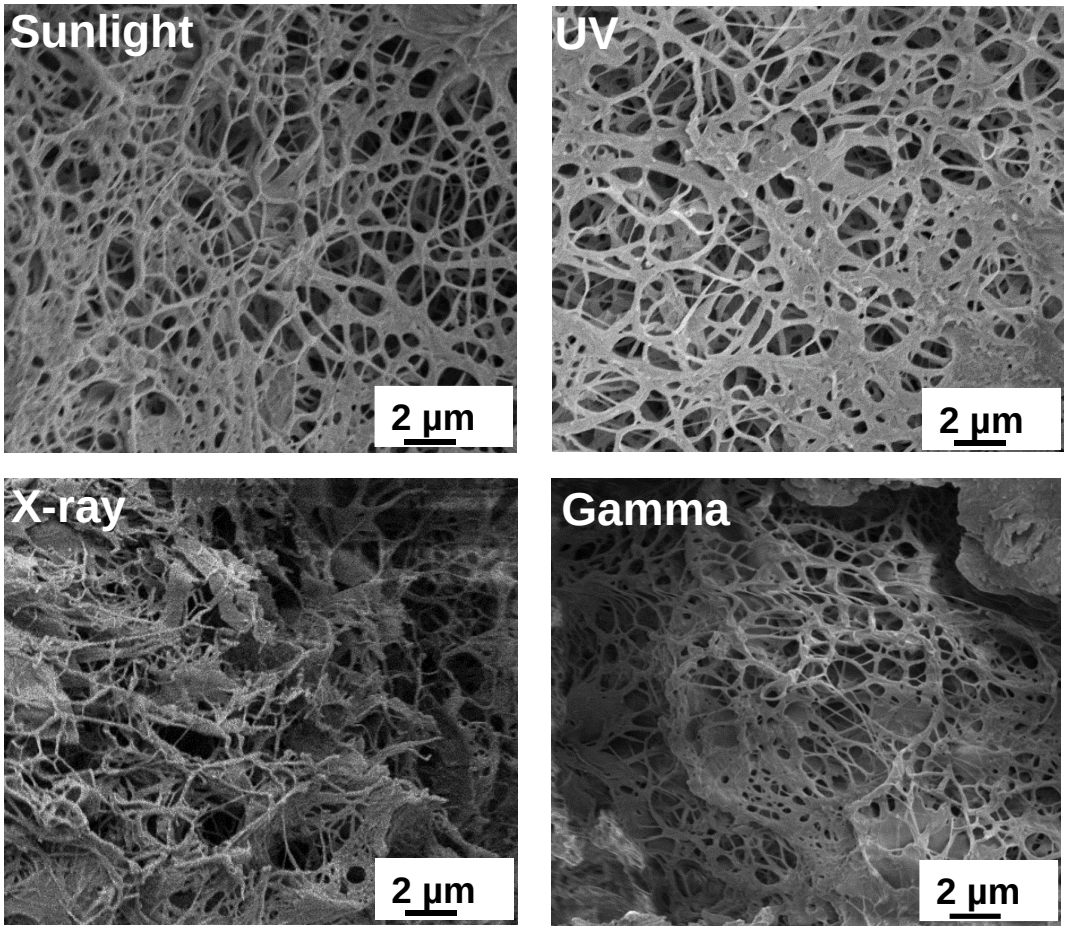

Figure S25: FESEM images, of PP-3 after exposure to different radiations.

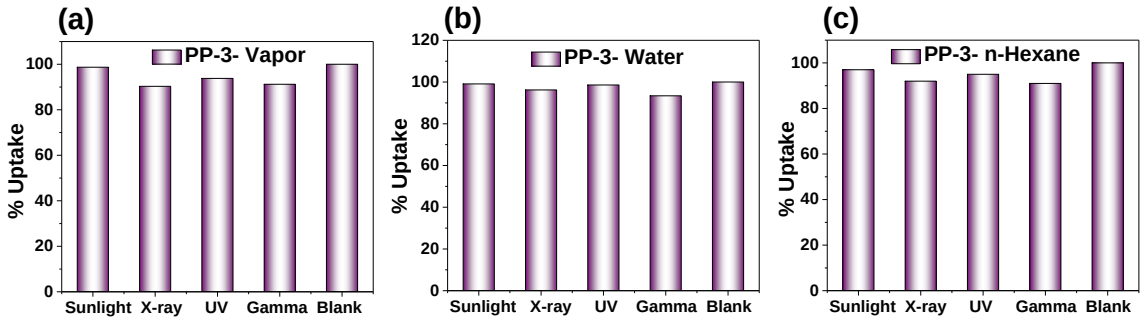

Figure S26: After exposure to different radiations, uptake percent of PP-3 for iodine adsorption in (a) vapor phase, (b) water, and (c) n-hexane.

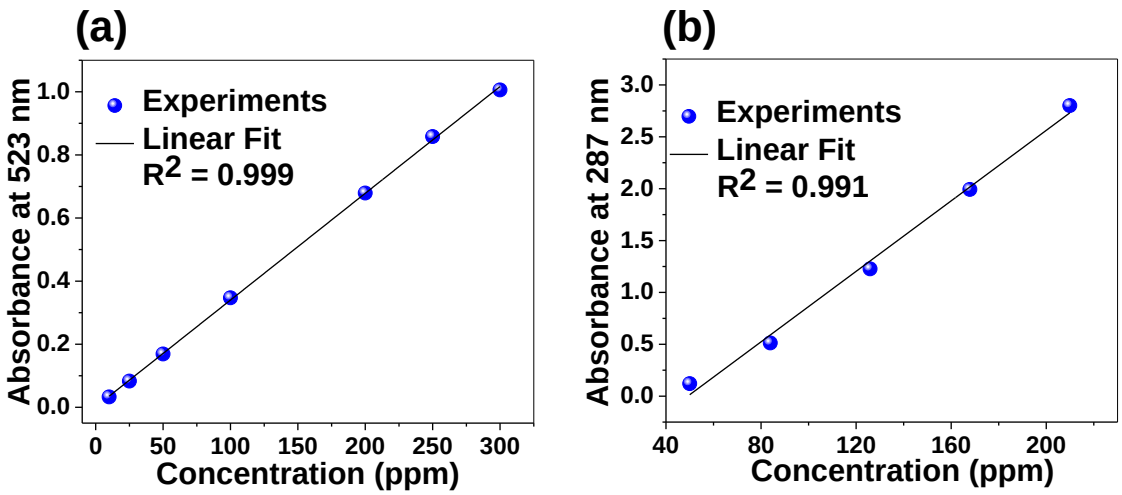

Figure S27: Iodine adsorption standard curves in (a) n-hexane and (b) water

References

1. RITTER, H. L., Pore-size disribution in porous materials. Pressure porosimeter and determination of complete macropore size distributions. *Ind. Eng. Chem., Anal. Ed.* **1945,** *17*, 782-786.
2. Washburn, E. W., Note on a method of determining the distribution of pore sizes in a porous material. *Proceedings of the National Academy of Sciences* **1921,** *7* (4), 115-116.
3. Bag, R.; Jadda, K., Influence of water content and dry density on pore size distribution and swelling pressure of two Indian bentonites. *Bulletin of Engineering Geology and the Environment* **2021,** *80* (11), 8597-8614.
4. Fathima, N. N.; Dhathathreyan, A.; Ramasami, T., Mercury intrusion porosimetry, nitrogen adsorption, and scanning electron microscopy analysis of pores in skin. *Biomacromolecules* **2002,** *3* (5), 899-904.
5. Ren, S.; Bojdys, M. J.; Dawson, R.; Laybourn, A.; Khimyak, Y. Z.; Adams, D. J.; Cooper, A. I., Porous, fluorescent, covalent triazine-based frameworks via room-temperature and microwave-assisted synthesis. *Advanced materials* **2012,** *24* (17), 2357-2361.
6. Zhu, X.; Tian, C.; Mahurin, S. M.; Chai, S.-H.; Wang, C.; Brown, S.; Veith, G. M.; Luo, H.; Liu, H.; Dai, S., A superacid-catalyzed synthesis of porous membranes based on triazine frameworks for CO2 separation. *Journal of the American Chemical Society* **2012,** *134* (25), 10478-10484.
7. Valizadeh, B.; Nguyen, T. N.; Smit, B.; Stylianou, K. C., Porous Metal–Organic Framework@ Polymer Beads for Iodine Capture and Recovery Using a Gas-Sparged Column. *Advanced Functional Materials* **2018,** *28* (30), 1801596.
8. Yao, S.; Fang, W.-H.; Sun, Y.; Wang, S.-T.; Zhang, J., Mesoporous assembly of aluminum molecular rings for iodine capture. *Journal of the American Chemical Society* **2021,** *143* (5), 2325-2330.
9. Guo, X.; Tian, Y.; Zhang, M.; Li, Y.; Wen, R.; Li, X.; Li, X.; Xue, Y.; Ma, L.; Xia, C., Mechanistic insight into hydrogen-bond-controlled crystallinity and adsorption property of covalent organic frameworks from flexible building blocks. *Chemistry of Materials* **2018,** *30* (7), 2299-2308.
10. Zhu, Y.; Qi, Y.; Guo, X.; Zhang, M.; Jia, Z.; Xia, C.; Liu, N.; Bai, C.; Ma, L.; Wang, Q., A crystalline covalent organic framework embedded with a crystalline supramolecular organic framework for efficient iodine capture. *Journal of Materials Chemistry A* **2021,** *9* (31), 16961-16966.
11. Dai, D.; Yang, J.; Zou, Y. C.; Wu, J. R.; Tan, L. L.; Wang, Y.; Li, B.; Lu, T.; Wang, B.; Yang, Y. W., Macrocyclic arenes-based conjugated macrocycle polymers for highly selective CO2 capture and iodine adsorption. *Angewandte Chemie* **2021,** *133* (16), 9049-9057.
12. Xu, M.; Wang, T.; Zhou, L.; Hua, D., Fluorescent conjugated mesoporous polymers with N, N-diethylpropylamine for the efficient capture and real-time detection of volatile iodine. *Journal of Materials Chemistry A* **2020,** *8* (4), 1966-1974.
13. Wang, P.; Xu, Q.; Li, Z.; Jiang, W.; Jiang, Q.; Jiang, D., Exceptional iodine capture in 2D covalent organic frameworks. *Advanced Materials* **2018,** *30* (29), 1801991.
14. Xie, Y.; Pan, T.; Lei, Q.; Chen, C.; Dong, X.; Yuan, Y.; Shen, J.; Cai, Y.; Zhou, C.; Pinnau, I., Ionic Functionalization of Multivariate Covalent Organic Frameworks to Achieve an Exceptionally High Iodine-Capture Capacity. *Angewandte Chemie International Edition* **2021,** *60* (41), 22432-22440.
15. Chang, J.; Li, H.; Zhao, J.; Guan, X.; Li, C.; Yu, G.; Valtchev, V.; Yan, Y.; Qiu, S.; Fang, Q., Tetrathiafulvalene-based covalent organic frameworks for ultrahigh iodine capture. *Chemical Science* **2021,** *12* (24), 8452-8457.

16. Geng, T.; Zhang, C.; Liu, M.; Hu, C.; Chen, G., Preparation of biimidazole-based porous organic polymers for ultrahigh iodine capture and formation of liquid complexes with iodide/polyiodide ions. *Journal of Materials Chemistry A* **2020,** *8* (5), 2820-2826.
17. Li, H.; Ding, X.; Han, B. H., Porous Azo-Bridged Porphyrin–Phthalocyanine Network with High Iodine Capture Capability. *Chemistry–A European Journal* **2016,** *22* (33), 11863-11868.
18. Li, G.; Yao, C.; Wang, J.; Xu, Y., Synthesis of tunable porosity of fluorine-enriched porous organic polymer materials with excellent CO2, CH4 and iodine adsorption. *Scientific reports* **2017,** *7* (1), 1-8.
19. Abdelmoaty, Y. H.; Tessema, T.-D.; Choudhury, F. A.; El-Kadri, O. M.; El-Kaderi, H. M., Nitrogen-rich porous polymers for carbon dioxide and iodine sequestration for environmental remediation. *ACS applied materials & interfaces* **2018,** *10* (18), 16049-16058.
20. Xiong, S.; Tang, X.; Pan, C.; Li, L.; Tang, J.; Yu, G., Carbazole-bearing porous organic polymers with a mulberry-like morphology for efficient iodine capture. *ACS applied materials & interfaces* **2019,** *11* (30), 27335-27342.
21. Qian, X.; Zhu, Z.-Q.; Sun, H.-X.; Ren, F.; Mu, P.; Liang, W.; Chen, L.; Li, A., Capture and reversible storage of volatile iodine by novel conjugated microporous polymers containing thiophene units. *ACS Applied Materials & Interfaces* **2016,** *8* (32), 21063-21069.
22. Du, W.; Qin, Y.; Ni, C.; Dai, W.; Zou, J., Efficient Capture of Volatile Iodine by Thiophene-Containing Porous Organic Polymers. *ACS Applied Polymer Materials* **2020,** *2* (11), 5121-5128.
23. Xu, Y.; Yu, H.; Shi, B.; Gao, S.; Zhang, L.; Li, X.; Liao, X.; Huang, K., Room-temperature synthesis of hollow carbazole-based covalent triazine polymers with multiactive sites for efficient iodine capture-catalysis cascade application. *ACS Applied Polymer Materials* **2020,** *2* (8), 3704-3713.
24. Zeng, M.-H.; Wang, Q.-X.; Tan, Y.-X.; Hu, S.; Zhao, H.-X.; Long, L.-S.; Kurmoo, M., Rigid pillars and double walls in a porous metal-organic framework: single-crystal to single-crystal, controlled uptake and release of iodine and electrical conductivity. *Journal of the American chemical society* **2010,** *132* (8), 2561-2563.
25. Li, G.; Yan, C.; Cao, B.; Jiang, J.; Zhao, W.; Wang, J.; Mu, T., Highly efficient I 2 capture by simple and low-cost deep eutectic solvents. *Green Chemistry* **2016,** *18* (8), 2522-2527.
26. Gogia, A.; Das, P.; Mandal, S. K., Tunable Strategies Involving Flexibility and Angularity of Dual Linkers for a 3D Metal–Organic Framework Capable of Multimedia Iodine Capture. *ACS Applied Materials & Interfaces* **2020,** *12* (41), 46107-46118.
27. Sen, A.; Sharma, S.; Dutta, S.; Shirolkar, M. M.; Dam, G. K.; Let, S.; Ghosh, S. K., Functionalized Ionic Porous Organic Polymers Exhibiting High Iodine Uptake from Both the Vapor and Aqueous Medium. *ACS applied materials & interfaces* **2021,** *13* (29), 34188-34196.
28. Wang, G.-Q.; Huang, J.-F.; Huang, X.-F.; Deng, S.-Q.; Zheng, S.-R.; Cai, S.-L.; Fan, J.; Zhang, W.-G., A hydrolytically stable cage-based metal–organic framework containing two types of building blocks for the adsorption of iodine and dyes. *Inorganic Chemistry Frontiers* **2021,** *8* (4), 1083-1092.
29. An, D.; Li, L.; Zhang, Z.; Asiri, A. M.; Alamry, K. A.; Zhang, X., Amino-bridged covalent organic polycalix [4] arenes for ultra efficient adsorption of iodine in water. *Materials Chemistry and Physics* **2020,** *239*, 122328.
30. Zhang, Z.; Li, L.; An, D.; Li, H.; Zhang, X., Triazine-based covalent organic polycalix [4] arenes for highly efficient and reversible iodine capture in water. *Journal of Materials Science* **2020,** *55* (4), 1854-1864.
31. Lin, Y.; Jiang, X.; Kim, S. T.; Alahakoon, S. B.; Hou, X.; Zhang, Z.; Thompson, C. M.; Smaldone, R. A.; Ke, C., An elastic hydrogen-bonded cross-linked organic framework for

effective iodine capture in water. *Journal of the American Chemical Society* **2017,** *139* (21), 7172-7175.
32. Zhao, Q.; Chen, G.; Wang, Z.; Jiang, M.; Lin, J.; Zhang, L.; Zhu, L.; Duan, T., Efficient removal and immobilization of radioactive iodide and iodate from aqueous solutions by bismuth-based composite beads. *Chemical Engineering Journal* **2021,** *426*, 131629.
33. Li, H.; Li, Y.; Li, B.; Liu, D.; Zhou, Y., Highly selective anchoring silver nanoclusters on MOF/SOF heterostructured framework for efficient adsorption of radioactive iodine from aqueous solution. *Chemosphere* **2020,** *252*, 126448.
34. Zheng, B.; Liu, X.; Hu, J.; Wang, F.; Hu, X.; Zhu, Y.; Lv, X.; Du, J.; Xiao, D., Construction of hydrophobic interface on natural biomaterials for higher efficient and reversible radioactive iodine adsorption in water. *Journal of hazardous materials* **2019,** *368*, 81-89.
35. Alsalbokh, M.; Fakeri, N.; Lawson, S.; Rownaghi, A. A.; Rezaei, F., Adsorption of iodine from aqueous solutions by aminosilane-grafted mesoporous alumina. *Chemical Engineering Journal* **2021,** *415*, 128968.
36. Xu, X.-H.; Li, Y.-X.; Zhou, L.; Liu, N.; Wu, Z.-Q., Precise fabrication of porous polymer frameworks using rigid polyisocyanides as building blocks: from structural regulation to efficient iodine capture. *Chemical Science* **2022**.